Effect of Lateral Constraint on the Mechanical Properties of a Closed-Cell Al Foam: Part II. Strain-Hardening Models

Effect of Lateral Constraint on the Mechanical Properties of a Closed-Cell Al Foam: Part II. Strain-Hardening Models

S. KARTHIKEYAN, M. KOLLURI, and U. RAMAMURTY

Experimental results, presented in the companion article, show that the compressive deformation of a closed-cell Al foam under lateral constraint is characterized by significant strain hardening. This enhanced hardening is due to the change in stress state from uniaxial to triaxial, which additionally contributes to friction between the deforming foam and the walls of the constraining sleeve. Detailed analysis, employing two different types of deformation models, is presented in this article in order to rationalize the experimental observations. In the heterogeneous model, it is assumed that plastic deformation is similar with and without constraint and that it occurs via collective plastic collapse of cells. The bands, thus formed, elastically bear the lateral stresses and give rise to friction. In the homogeneous deformation model, it is assumed that the deformation mode is different under constraint and involves uniform densification, which leads to inherent hardening as well as additional friction. By comparing the model predictions with experimental observations, it is suggested that the plastic strain hardening of the metallic foam under constraint is due, in equal measure, to the triaxial state of stress and friction. Mechanistically, the material deforms principally by collective cell collapse, though there is some evidence of concurrent homogeneous deformation.

DOI: 10.1007/s11661-007-9213-7

I. INTRODUCTION

IN a companion article, it was shown that the mechanical response of aluminum foams is different when compression tested with and without constraint.[1] In particular, specimens tested with lateral constraint were observed to exhibit a higher strain-hardening rate than samples tested without. The implications of such hardening on densification strains, energy absorbed, and the fatigue properties were also explored. Clearly, an in-depth understanding of the causes and effects of hardening under constraint is of scientific and technological significance. Macrographs of samples deformed under constraint shown in Figure 5 (a) (Part I) reveal similarities as well as differences in the deformation micromechanisms with and without constraint.[1] Analytical constitutive models that rationalize the observed strain hardening are developed in this article, with a view to explore the possible sources of hardening.

Two possible sources can be considered for the experimentally observed strain hardening in foam specimens tested under lateral constraint, as seen in Figure 4 (b) (Part I).[1] The application of the constraint prevents Poisson expansion and fundamentally changes the stress state from uniaxial to triaxial. This is expected to *intrinsically* affect deformation in the foam leading to strain hardening. The second possible source of hardening is *extrinsic* in the form of friction between the die steel sleeve and foam surface, which contributes to the stress required to deform the specimen. In the following sections, we will discuss these causes for hardening and develop a framework for modeling the observed behavior.

S. KARTHIKEYAN, Assistant Professor, M. KOLLURI, Master of Engineering Student, and U. RAMAMURTY, Associate Professor, are with the Department of Materials Engineering, Indian Institute of Science, Bangalore 560012, India. Contact e-mail: ramu@materials.iisc.ernet.in

Manuscript submitted November 20, 2006.
Article published online July 20, 2007.

II. INTRINSIC STRAIN HARDENING DUE TO MULTIAXIALITY

A. *Background*

Plastic deformation in metal foams occurs through the collective collapse of cells, with the bands typically perpendicular to loading direction.[2] This local deformation propagates from one band to another progressively, until all the cells are collapsed, leading to the plateau region in the stress-strain curve.[3–6] This is followed by a rapid stress rise with further strain corresponding to densification. However, as pointed out in Part I, different aluminum foams exhibit marginal to significant hardening and thus deviate from the perfect plateau behavior even in the absence of constraint.[7] Kenesei *et al.* attributed this hardening to structural variability, which causes the collapse of progressively stronger cell bands leading to the observed macroscopic hardening.[8] However, Figures 2 and 4(b) in Part I reveal very small strain hardening rates without constraint for the ALPORAS foams under consideration.[1] This observation is not completely unexpected. During deformation involving collective collapse, horizontal structural variability about a collapsed strut is of little consequence, and the overall effect of variability on hardening is minor.

While explicit studies on the effect of constraint on the plastic properties of metal foams have not been conducted, several researchers have looked into multiaxial deformation[9–13] with the aim of developing appropriate models for the yield surface of metal foams. The general conclusion of these studies is that macroscopic yielding of the metal foam is delayed to higher stresses under multiaxial/hydrostatic loading. Gibson *et al.*[4] have suggested that the bending moments on the struts are largely suppressed in multiaxial loading, unlike in the uniaxial loading wherein bending stresses on the struts are significant. Consequently, for foams of relative density ~0.1, there is a change in the deformation mode from bending of plastic hinges to axial deformation of struts, when the stress state changes from uniaxial to multiaxial. We have confirmed this hypothesis by doing a finite element truss analysis on a 2d honeycomb structure that was compressed with and without constraint. The constraint, as expected, makes the stress state multiaxial.

The mechanistic model from Gibson *et al.* has been observed to significantly overpredict yield stress, particularly under triaxial loading. This is because it does not account for structural imperfections that induce bending even under multiaxial loading. Studies on the effect of structural defects reveal that cell wall waviness and curvature play an important role in determining the yield surface.[10,14–16] Gioux *et al.* have included the effect of these imperfections and have predicted a yield surface that matches well with experimental data.[10] Our observations on the plastic strength, its dependence on density (Figure 4(a), Part I), and the role of constraint also underscore the significance of imperfections.[1] Remarkably, the plastic strength is similar with and without constraint. Moreover, the plastic strength shows a power-law dependence on relative density with an exponent of 1.5. Such an exponent is thought to correspond to the plastic deformation micromechanism where bending of cell edges dominates.[4] These observations suggest that the deformation micromechanisms, with and without constraint, are largely similar with cell edge bending as the dominant component. One could conclude that, while multiaxiality increases the plastic strength, the effect is diluted because of foam imperfections.

Enhanced strain hardening under multiaxial loading has been previously reported.[9,11] Deshpande and Fleck[9] have proposed two constitutive models for strain hardening under such conditions. In this context, they have developed a phenomenological yield surface model that takes into account the dependence of yield on the deviatoric and hydrostatic stress components. The latter comes into the picture because volume is not conserved during plastic deformation of foams. A geometrically self-similar evolution of the yield surface (with equivalent strain) is invoked in the first strain-hardening model, while the second allows for a change in shape of the yield surface due to differential hardening for the deviatoric and hydrostatic components. The Deshpande and Fleck (DF) constitutive model, as well as other models, including those developed by Miller *et al.*[11] and Zhang *et al.*,[17] incorporate the plastic Poisson's ratio (defined as the ratio of radial to axial plastic strain rate in an axisymmetric test[9]) in the hardening law.

The aim of this work is to model strain hardening in metal foams under constraint, *i.e.*, to physically model the yield surface evolution with strain. Therefore, no attempt is made to develop a yield surface model. Instead, the functional form of the extant DF model is used for describing the yield surface.[9] The advantage of this model lies in its simplicity and its dependence on a readily measurable microstructural parameter. In Section B, we will review the DF yield surface model. In Section IV, we describe how the yield surface evolves if one were to incorporate a model for evolution of foam structure with strain.

B. *The DF Model*

During the initial elastic deformation, the constraint prevents elastic Poisson expansion in the transverse direction (labeled 2 and 3) due to the application of a compressive σ_1. This leads to the development of transverse compressive stresses, σ_2 and σ_3, which in turn lead to longitudinal expansive strains along the 1 direction. Assuming that the metal foam is transversely isotropic, the elastic constitutive law is given by

$$\sigma_2 = \sigma_3 = \left(\frac{v_e}{1 - v_e}\right)\frac{E_2}{E_1}\cdot \sigma_1 \qquad [1]$$

where E_1 and E_2 are the longitudinal and transverse elastic moduli, and v_e is the elastic Poisson ratio (assumed to be invariant with the orientation).

The DF yield criterion for metallic foams is given as

$$\sigma_{p,0}^2 = \frac{1}{\left[1 + (\alpha/3)^2\right]}\left[\sigma_e^2 + \alpha^2\sigma_m^2\right] \qquad [2]$$

where $\sigma_{p,0}$ is the uniaxial unconstrained flow stress at zero plastic strain, σ_e is the von Mises effective stress, σ_m is the mean stress, and α is a parameter that determines the ellipsity of the yield locus and is related to the plastic Poisson's ratio, v_p, *via*

$$v_p = \frac{0.5 - (\alpha')^2}{1 + (\alpha')^2} \qquad [3]$$

where $\alpha' = \alpha/3$. When $\alpha = 0$ and $v_p = 0.5$ (*i.e.*, complete volume conservation), the DF criterion given by Eq. [2] resolves to the von Mises criterion. So, α also determines the extent to which the hydrostatic stresses affect the yield surface and is a measure of volume constancy during plastic deformation of the foam.[9]

The yield criterion per Eq. [2] may be rewritten in terms of the principal stresses:

$$\sigma_2 = \sigma_3 = \frac{\left(1 - 2\cdot\alpha'^2\right)}{\left(1 + 4\cdot\alpha'^2\right)}\sigma_1 \pm \frac{\sqrt{\left(1 + 5\cdot\alpha'^2 + 4\alpha'^4\right)\cdot\sigma_{p,0}^2 - 9\cdot\alpha'^2\sigma_1^2}}{\left(1 + 4\cdot\alpha'^2\right)} \qquad [4]$$

Figure 1 shows the yield surface in the σ_1 and σ_2 space for a specific ALPORAS foam with relative density of

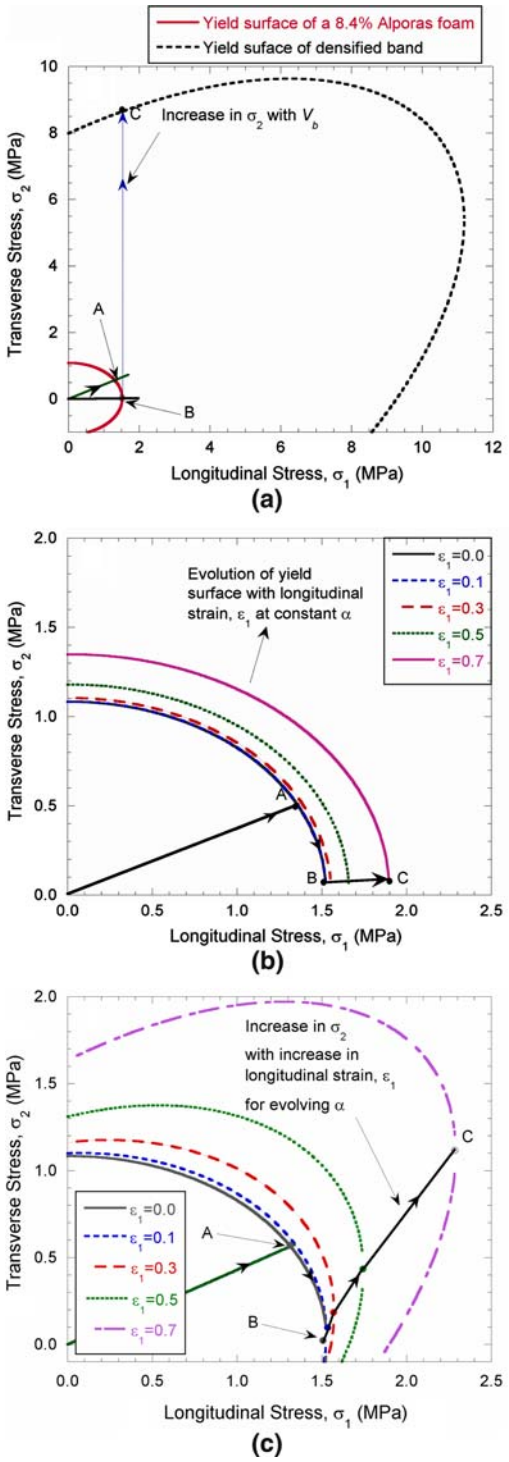

Fig. 1—(*a*) Yield surface for foam (relative density of 8.4 pct) is shown alongside the yield surface for a densified band (relative density of 28 pct). The figure also schematically shows the evolution of the stress-state during heterogeneous deformation. The increase in σ_2 is due to the increase in the volume fraction of bands. The heterogeneous model also assumes the self-similar evolution (*i.e.*, constant α) of the smaller ellipse. For clarity, this evolution is not represented in the schematic. (*b*) Progress of the stress state if the yield surface evolved in a self-similar manner. (*c*) Stress-state evolution when α is also assumed to evolve with strain. In all of the schematics, point A represents the initiation of yield, while B represents the equilibrium (relaxed) stress state, and point C corresponds to the stress state at some plastic strain.

8.4% for which Deshpande and Fleck have deduced that $\alpha = 2.08$.[9] Note that the compressive stresses have been plotted in the first quadrant for simplicity.

Prior to plastic deformation, the material is isotropic, so $E_1 = E_2$. Additionally, metal foams typically have an elastic Poisson's ratio close to 0.3.[4] So, from Eq. [1] and for $v_e = 0.3$, we obtain a stress ratio, $\beta_A = \sigma_2/\sigma_1 = 0.429$. The σ_1 at this stress ratio is the constrained yield strength. Figure 1 shows where plastic deformation begins (point A) and probable deformation paths that may be followed by the metal foam during subsequent plastic deformation. Point B in Figure 1 represents a unique stress state (σ_1^B, σ_2^B) on the yield surface. On the yield surface, if $\sigma_2 > \sigma_2^B$, the normality condition requires that the transverse plastic strain, $\varepsilon_{2,\text{plastic}}$, has the same direction as σ_2. Because the elastic transverse strain is along the negative σ_2 direction, it is opposed by $\varepsilon_{2,\text{plastic}}$ leading a relaxation of the compressive stress. Similarly, if $\sigma_2 < \sigma_2^B$, $\varepsilon_{2,\text{plastic}}$ has the opposite direction as σ_2 due to which the plastic and elastic transverse strains add up leading to an increase in σ_2. At point B, these two strains are perfectly balanced and represent the equilibrium value of σ_2 required for sustained yielding with constraint.

For this reason, initial yielding at point A (where $\sigma_2 > \sigma_2^B$) leads to the complete relief of elastic strain by plastic strain along the transverse direction, as indicated in Figure 1 between the points A and B. Again invoking the normality condition, one infers that point B on the yield surface is determined by $d\varepsilon_2/d\varepsilon_1 = -d\sigma_1/d\sigma_2 = 0$. This leads to $\beta_B = \sigma_2/\sigma_1 = \left(1 - 2\cdot\alpha'^2\right)/\left(1 + 4\cdot\alpha'^2\right)$ and $\sigma_1 = \sqrt{\left(1 + 5\alpha'^2 + 4\alpha'^4\right)}\cdot\sigma_{p,0}/3\alpha'$. As the material hardens ($\sigma_p > \sigma_{p,0}$) and the yield surface expands, the stress state at yield (under constraint) is governed by the condition $d\sigma_1/d\sigma_2 = 0$.

III. EXTRINSIC HARDENING DUE TO FRICTION

During the conduction of experiments with constraint, it was observed that samples could be slid into the steel sleeve with relative ease before the test, whereas a significant force was needed to remove them after the test. This suggests that friction between the steel sleeve and the foam could be an important factor determining the apparent stress needed for deforming the sample under constraint. Thus, it is imperative that the friction stress be accounted for in rationalizing the observed strain hardening.

The contacting surfaces of the foam and the sleeve move relative to each other during the test, and this motion is opposed by frictional forces that develop because of the transverse compressive stress, σ_2, due to constraint. This friction force increases the load required to plastically deform the specimen, and additionally contributes to the positive slope. For a specimen of square cross section with cross-sectional dimension, w, initial height, L_0, and instantaneous

height, L, the normal force on each of the two walls in the 2 direction is

$$F_2 = \frac{1}{2}\sigma_2 \cdot L \cdot w \qquad [5]$$

The friction force (per face) along the 1 direction is given by $f_{\text{friction}} = \mu F_2$, where μ is the friction coefficient. The total friction force on the four faces for this specimen with square cross section is

$$F_{\text{friction}} = 4 \cdot f_{\text{friction}} = 2 \cdot \mu \cdot \sigma_2 \cdot L \cdot w \qquad [6]$$

During plastic deformation, the total force (in the 1 direction) required to cause plastic flow and to overcome friction, is given by

$$F_{1,\text{total}} = F_{1,\text{plastic}} + F_{\text{friction}} = F_{1,\text{plastic}} + 2 \cdot \mu \cdot \sigma_2 \cdot L \cdot w. \qquad [7]$$

This can be equivalently expressed as the total compressive stress for plastic deformation:

$$\sigma_{1,\text{total}} = \frac{F_{1,\text{total}}}{w^2} = \sigma_{1,\text{plastic}} + 2 \cdot \mu \cdot \sigma_2 \cdot \left(\frac{L}{w}\right) \qquad [8]$$

Note that L, at strain, ε, is related to L_0, *via* $L = L_0(1-\varepsilon)$ and this leads to

$$\begin{aligned}\sigma_{1,\text{total}} &= \sigma_{1,\text{plastic}} + 2 \cdot \mu \cdot \sigma_2 \cdot \left[\frac{L_0(1-\varepsilon)}{w}\right] \\ &= \sigma_{1,\text{plastic}} + 2 \cdot \mu \cdot \sigma_2 \cdot R \cdot (1-\varepsilon)\end{aligned} \qquad [9]$$

where $R = (L_0/w)$ is the initial sample aspect ratio.

Equation [9] gives the relation between flow stress and strain and highlights the two fundamental sources of hardening: the inherent increase in the flow stress due to triaxiality (as reflected in the change in $\sigma_{1,\text{plastic}}$) and additional stress due to friction. The friction contribution indirectly depends on the stress state *via* σ_2. The equation suggests an apparent drop in the stress with strain, *i.e.*, strain softening. However, in Section IV, it will be shown that the increase in σ_2 with strain comfortably offsets such a drop.

IV. HOMOGENEOUS *vs* HETEROGENEOUS DEFORMATION

In Sections A and B, two models are considered for rationalizing the hardening behavior under constraint. They describe two distinct and extreme cases of evolution of foam structure (with strain) and represent the heterogeneous or homogeneous deformation of the foam.

A. *Heterogeneous Deformation Model*

As mentioned in Section II, when metallic foams are deformed without constraint, plastic deformation localizes as bands that are typically perpendicular to the loading direction. This results in the conversion of low density foam into a series of high density bands separated by virgin foam. Without constraint, the formation of bands perpendicular to the loading axis has little effect on the flow stress. If this micromechanism of deformation is assumed to be invariant with the type of loading, transverse elastic stresses develop when deformation is laterally constrained due to the inhibition of the elastic Poisson expansion of the bands. This is based on the assumption that the high density bands have a higher flow stress compared to the foam, and so they carry the load elastically while the foam continues to deform plastically. Continued deformation leads to an increase in the volume fraction of material in bands due to which the load borne elastically by the bands increases (i.e., σ_2 increases with strain). This, in turn, causes an increase in friction with strain leading to strain hardening.

Because the specimen is assumed to deform subsequently in a manner akin to a laminated composite, the mean transverse stress, σ_2, experienced by the foam can be found using an isostrain assumption:

$$\sigma_2 = V_b \cdot \sigma_{2,\text{elastic}} + V_f \cdot \sigma_{2,\text{plastic}} \qquad [10]$$

where V_b and V_f are the volume fractions of material in bands or as foam, respectively. Note that $\sigma_{2,\text{elasic}}$ is the transverse elastic stress in the bands and $\sigma_{2,\text{plastic}}$ corresponds to σ_2 on the yield surface. Using Eq. [1] for $\sigma_{2,\text{elastic}}$ and noting that, along the 1 direction, $\sigma_{1,\text{elastic}} = \sigma_{1,\text{plastic}}$ due to the isostress state, we obtain

$$\sigma_2 = V_b \cdot \left(\frac{v_e}{1-v_e}\right)\frac{E_2}{E_1} \cdot \sigma_{1,\text{plastic}} + V_f \cdot \sigma_{2,\text{plastic}} \qquad [11]$$

The essence of the heterogeneous model is shown schematically in Figure 1(a).

One could use mass conservation to determine the volume fractions of material in the band and in the foam as a function of strain. The densification of an elemental width, dl_f, of foam (initial density, ρ_f) leads to the gain of a band of density ρ_b and elemental width dl_b:

$$\rho_f \cdot A \cdot dl_f = -\rho_b \cdot A \cdot dl_b \qquad [12a]$$

from which we have

$$\rho' \equiv \frac{\rho_f}{\rho_b} = -\frac{dl_b}{dl_f} \qquad [12b]$$

Using Eq. [12], the incremental change in length due to compression can be written as

$$dL = dl_f + dl_b = \left(1 - \frac{1}{\rho'}\right) \cdot dl_b \qquad [13]$$

Integrating both sides of Eq. [13] from L_0 to L and dividing by L, we obtain

$$1 - \frac{L_0}{L} = \left(1 - \frac{1}{\rho'}\right) \cdot \frac{l_b}{L} = \left(1 - \frac{1}{\rho'}\right) \cdot V_b \qquad [14]$$

where l_b, is the total width of the densified banded material and $V_b = l_b/L$, is the instantaneous volume

fraction of the material in bands. Using Eq. [14], one could calculate V_b as a function of the instantaneous length, L. Because $L = L_0 \cdot (1-\varepsilon)$, Eq. [14] may be rewritten as

$$1 - \frac{1}{1-\varepsilon} = \left(1 - \frac{1}{\rho'}\right) \cdot V_b \qquad [15]$$

On simplifying, one obtains

$$V_b = \frac{\varepsilon \cdot \rho'}{(1-\varepsilon)(1-\rho')} \qquad [16a]$$

$$V_f = 1 - \frac{\varepsilon \cdot \rho'}{(1-\varepsilon)(1-\rho')} = \frac{(1-\varepsilon-\rho')}{(1-\varepsilon)(1-\rho')} \qquad [16b]$$

Clearly, the volume fraction of material in bands increases with increasing strain.

The high-density bands also have a higher transverse elastic modulus *vis-à-vis* the less dense foam. Thus, the elastic properties of the foam are no longer isotropic. One could use a rule-of-mixtures approach to find the transverse elastic modulus, E_2, of the foam with bands:

$$E_2 = V_b \cdot E_b + V_f \cdot E_f \qquad [17]$$

where E_b and E_f are the elastic moduli of the material in bands or as foam, respectively. Increasing volume fraction of bands should lead to an increase in the transverse elastic modulus, E_2, with strain. This result is also confirmed by experiments. Transverse modulus measurements were made at different longitudinal strains. In these experiments, the specimen was deformed along the longitudinal direction up to a specific strain level under constraint. Then the specimen was removed from the sleeve and loaded and unloaded in the transverse direction elastically, and the slope of these curves was taken to be E_2. The evolution of E_2 with strain is shown in Figure 2. For a foam of relative density 0.1, we obtain E_b = 1223 MPa, E_f = 526 MPa, and $\rho' \equiv \rho_f/\rho_b = 0.3$ by fitting the experimental data to Eqs. [16] and [17]. Further measurements are underway to quantify these parameters as a function of initial foam density. In the present context, we assume that ρ' is constant and independent of the density of the foam. The value of σ_2 from Eq. [11] can be used in conjunction with Eqs. [9] and [17] to obtain the value of the total macroscopic stress σ_1 as a function of strain.

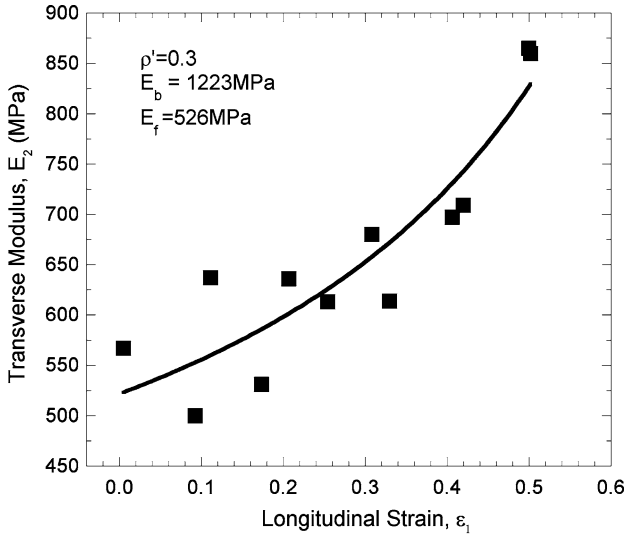

Fig. 2—Increase in the transverse modulus is shown as a function of longitudinal plastic strain. The fitted values of E_b, E_f, and ρ' are indicated.

B. *Homogeneous Deformation Model*

In the previous model, deformation was assumed to be localized to undeformed foam, while the higher density bands remained largely elastic. The chief source of the observed hardening was attributed to friction. Even before quantitatively testing the accuracy of the previous model, it should be mentioned that it is not entirely satisfactory for several physical reasons. First, the stress state with constraint is not uniaxial. Therefore, the predilection for plastic localization *via* band formation perpendicular to the uniaxial loading axis is diminished. As mentioned in Section II–A, collective cell collapse is a result of plastic hinge formation under bending stresses. Under constraint, bending stresses are suppressed and this makes band formation more difficult. One can understand this by realizing that in the absence of a principal uniaxial loading direction, there is little preference for one specific direction for band formation. This is also verified by visual examination of samples tested under constraint (Figure 5, Part I), which does not reveal extensive banding. Even when bands are formed, they are at 75 deg to the loading axis and not perpendicular.

Second, as shown in Figure 6 (a) (Part I), the densification strain is marginally but measurably lesser for the constrained case for all densities. This result suggests that the application of constraint has the effect of preponing the densification process. One can only conclude that this is because of continued densification of the foam during plastic deformation under constraint. The heterogeneous model, in which the deformation mechanism is unchanged for the constrained and unconstrained cases, cannot predict this premature onset of densification.

Finally, a material with $\nu_p = 0$ is sensitive to hydrostatic stresses but does not display a plastic Poisson effect. A material with $\nu_p = 0.5$ behaves in an exactly opposite way. The intermediate values observed in metal foams (including ALPORAS) allow for both plastic Poisson's effects and sensitivity to hydrostatic stresses. In this context, the inherent hardening of the foam under the triaxial stress state has to be rethought.

In the homogeneous deformation model, we assume that plastic deformation under constraint is accommodated not by localized densification in the bands, but by homogeneous densification of foam. The stress required for continued deformation is determined by the evolution of the yield surface. As discussed in Section II, the

stress state that satisfies the yield criterion for a given value of σ_p is

$$\sigma_{1,\text{plastic}} = \sqrt{(1 + 5\alpha'^2 + 4\alpha'^4)} \cdot \frac{\sigma_p}{3\alpha'} \qquad [18a]$$

$$\sigma_{2,\text{plastic}} = \beta\sigma_1 = \frac{(1 - 2 \cdot \alpha'^2)}{(1 + 4 \cdot \alpha'^2)}\sigma_1 \qquad [18b]$$

Because σ_p increases with strain (as evidenced by the finite, albeit small, strain-hardening rate in the unconstrained case) $\sigma_{1,\text{plastic}}$ and $\sigma_{2,\text{plastic}}$ are also expected to increase, thus leading to both inherent hardening and frictional hardening (*via* Eq. [11] with $\sigma_{2,\text{plastic}}$ instead of σ_2). The dependence of σ_p on the equivalent strain, $\hat{\varepsilon}$, may be elicited from the unconstrained tests. Using this hardening law and Eq. [18], one can track how $\sigma_{1,\text{plastic}}$ and $\sigma_{2,\text{plastic}}$ evolve with equivalent strain and this in turn can be related to the axial strain in the DF model by[9]

$$\varepsilon_1 = \hat{\varepsilon}\frac{\left(1 + \alpha^2\eta/3\right)}{\sqrt{(1 + \alpha^2\eta^2) \cdot (1 + \alpha'^2)}} \qquad [19]$$

where $\eta \equiv \left|\frac{\sigma_m}{\sigma_e}\right|$. At yield, $\eta = \left|\frac{(1+2\beta)}{3(1-\beta)}\right|$ for the present case.

The dependence of $\alpha' = \alpha/3$ on strain is also important. If α' remained constant, then the yield surfaces at different strains would look self-similar (Figure 1(b)). The strain hardening accomplished by such a self-similar hardening path has been found to be minimal. Moreover, the assumption of α' constancy is questionable for the following reason. When the material deforms homogeneously under constraint, it densifies. The density, ρ_c, corresponding to a certain axial strain, is given by $\rho_c = \rho^*/1 - \varepsilon_1$, where ρ^* is the relative density of the undeformed foam. As ρ_c increases with strain, it becomes increasingly difficult for hydrostatic stresses to densify it further. This implies that with increasing strain, there is an increase in v_p and a decrease in α, which is related to v_p *via* Eq. [3]. When complete densification is achieved, v_p reaches its maximum value of 0.5. This increase in v_p corresponds to the gradual change in the shape of the yield surface from nearly circular to the elliptical von Mises yield surface. Experimental data culled from literature and from our experiments confirm that, as the density of the foam increases, the value of α decreases, as shown in Figure 3. Note that the α values shown have been taken from both undeformed foams and foams deformed to specific strains, and the data appear to fall along the same master curve. A logarithmic fit appears most appropriate in describing available data. Figure 1(c) schematically shows the evolution of the yield surface and the stress state for plastic deformation under the homogeneous deformation assumption with an evolving value of α. Equations [18] and [19], in conjunction with the evolving value of α from Figure 3, lead to the modified hardening law for homogeneous deformation.

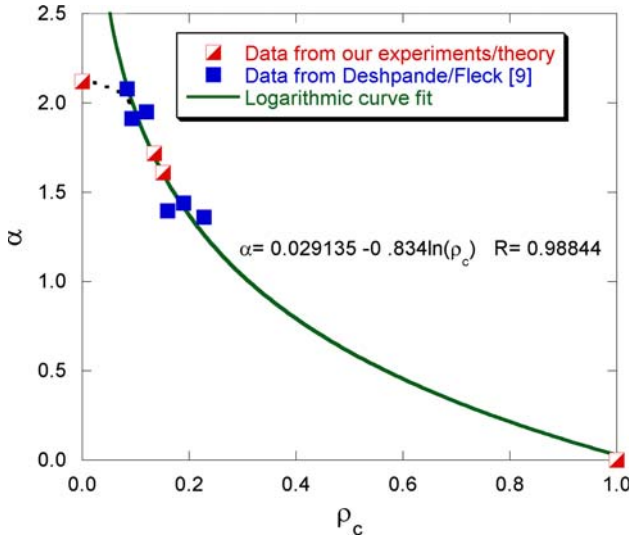

Fig. 3—Dependence of α on the current relative density of the foam is shown. The indicated logarithmic fit appears to best represent the data.

V. PREDICTIONS AND COMPARISON WITH EXPERIMENTAL RESULTS

Both models require the determination of the friction coefficient. Due to the size of cells in the foam and the fact that contact between the sleeve and the foam is planar, a flat-on-flat configuration (instead of the pin-on-disk) was used to determine the friction coefficient. The inset in Figure 4 shows a schematic of the friction measurement setup. A flat block of foam (100-mm thick with 600×500 mm^2 cross section) was held inclined at a fixed angle with the help of a support, and a die steel plate (14-mm thick with 50×50 mm^2) was slid down

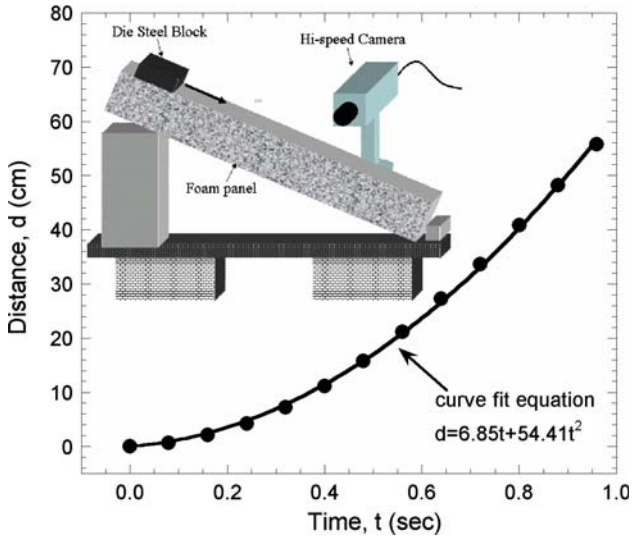

Fig. 4—Typical distance *vs* time plot obtained from the sliding friction experiments. The inset shows a schematic of the friction measurement setup. The friction coefficient thus obtained was found to be independent of the sliding velocities encountered in this setup.

the incline under the influence of gravity. The angle of inclination, θ, was chosen to ensure that static friction was overcome. Sliding was video recorded with the help of a Motion Scope M1 high-speed camera (Redlake MASD LLC, USA) at a rate of 125 frames/s. By placing markers on the foam block and die steel plate, the distance traveled by the die steel plate is recorded as a function of time. Figure 4 shows one such distance-time plot. The acceleration of the die steel block was calculated from the distance-time plot. This test was repeated several times and at several angles of inclination. The friction coefficient was derived from this acceleration, a, using $\mu = \left(\tan\theta - \frac{a}{g\cos\theta}\right)$. The friction coefficient was found to be ~0.3.

The predictions of the two models are shown in Figures 5 through 8. Figure 5 compares the stress-strain curve for the constrained sample of relative density 0.1 and shows the predictions of the two models. The contributions of both inherent hardening and that with friction are shown. Both models predict the evolution of flow stress under constraint reasonably well, and simply based on Figure 5, one cannot conclude if one model fits the data better than the other. However, it is apparent that without friction the experimentally observed strain hardening is not achieved in either model. The role of friction on the observed strain hardening is significant. Figure 6(a) shows the stress-strain curves and predictions of the heterogeneous model for different relative densities. Figure 6(b) is a similar plot for the homogeneous model. The heterogeneous model predicts a nearly linear plastic stress-strain dependence, whereas the homogeneous model predicts an accelerating stress-strain curve. At large strains, the homogeneous model

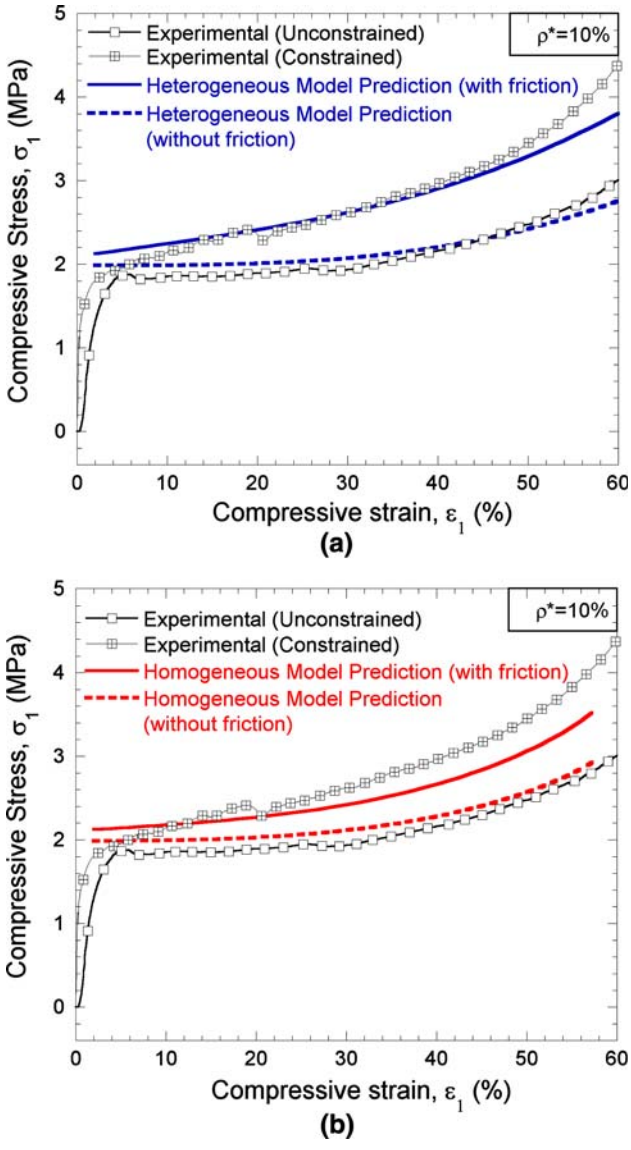

Fig. 5—Stress-strain curves for the unconstrained and constrained cases are compared against (*a*) the heterogeneous model and (*b*) the homogeneous model. Clearly, frictional contribution is important to rationalize the observed strain hardening behavior in both models.

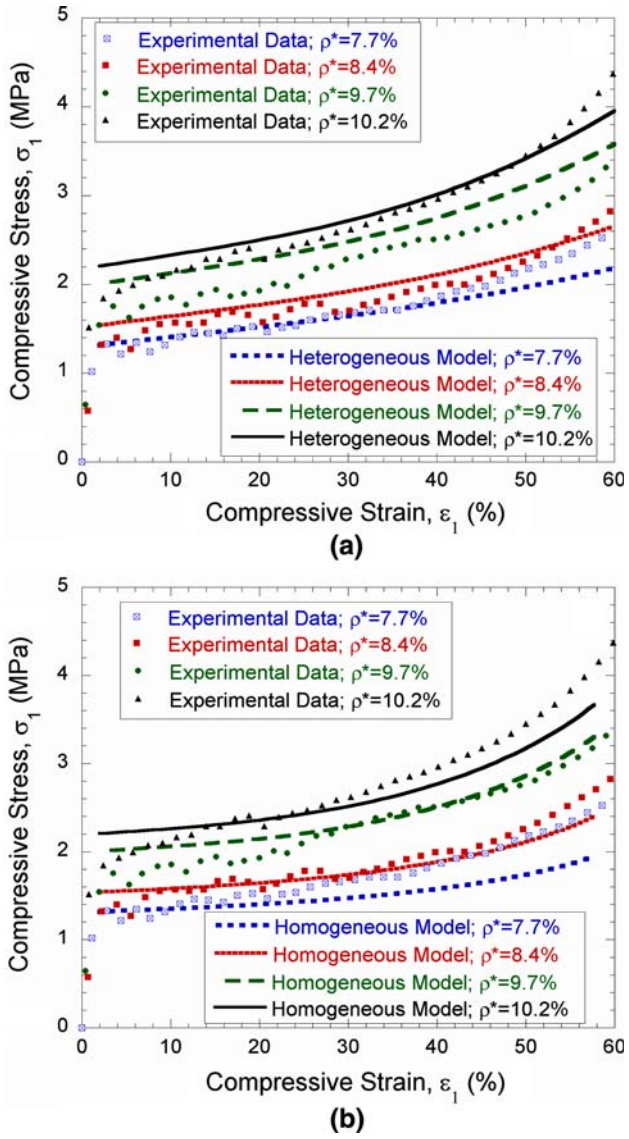

Fig. 6—Effect of relative density on the stress-strain curves in the constrained case is compared with (*a*) the heterogeneous model and (*b*) the homogeneous model.

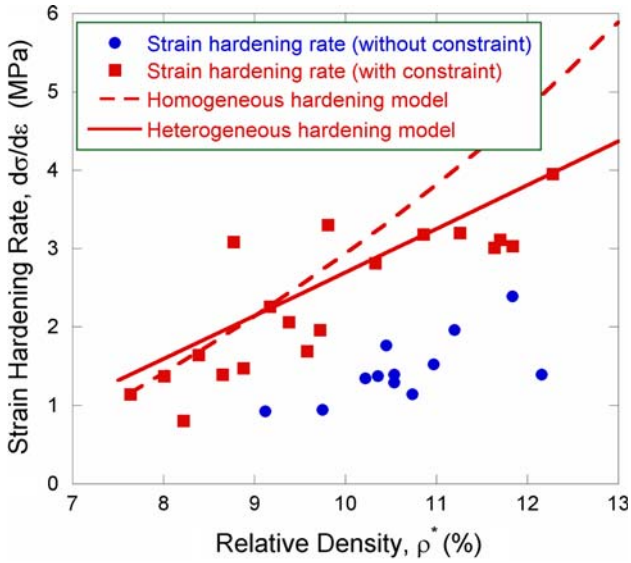

Fig. 7—The strain-hardening rate obtained by experiment and predicted by the two models are compared for the constrained case. The strain hardening rate for the unconstrained case is also shown for contrast.

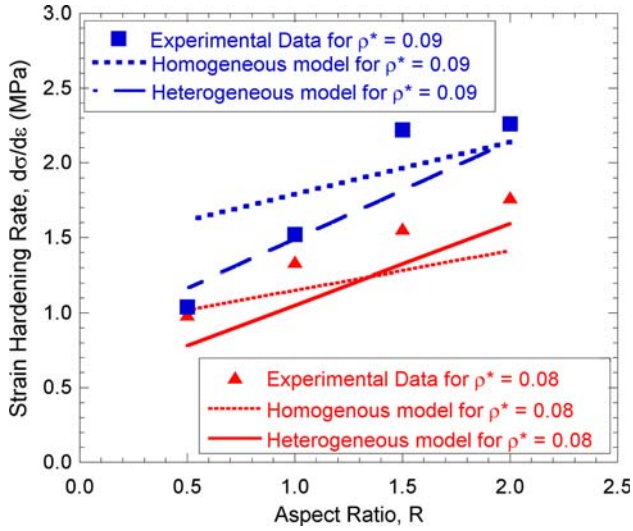

Fig. 8—Dependence of the strain-hardening rate of the specimen aspect ratio is indicated for specimens of two initial relative densities. Also shown are the model predictions.

predicts premature densification. Figure 7 is a plot of the strain-hardening rate (as defined in Section III–C, Part I) as a function of relative density. Both models predict a higher strain hardening rate for the constrained case and both predict steeper density dependence than for the unconstrained case. While both models slightly overpredict the strain hardening rate, the deviation is greater for the homogeneous model, particularly at higher densities. The density dependence of the strain hardening rate predicted by the heterogeneous model is definitely a better fit.

As mentioned earlier, friction clearly seems to play an important role in determining the observed strain hardening rate. To probe this aspect further, compression tests were conducted on samples with different aspect ratios, R. Note that both deformation models have a linear dependence of stress on the specimen aspect ratio. Samples of 25-, 50-, 75-, and 100-mm heights and 50×50 mm cross section were tested with constraint. These tests were conducted on samples with two different relative densities. The strain hardening rates measured from the experiments (Figure 8) clearly show a direct dependence on the aspect ratio, further strengthening the friction argument. The model predictions are also shown for comparison. Figure 8 reveals that, for both densities, the steep dependence of the strain-hardening rate on aspect ratio is better predicted by the heterogeneous model than the homogeneous model. Other aspects related to the model are discussed briefly in Section VI.

VI. DISCUSSION

The two models embody two distinct deformation modes and represent the qualitative limiting cases. Even though Figures 7 and 8 lend support to the heterogeneous deformation hypothesis, the general model predictions from the last section do not conclusively favor this mechanism *vis-à-vis* homogeneous deformation. In this section, we look for other evidence that would allow us to isolate the operating mechanism.

Experiments were carried out to directly measure the magnitude of the friction force. In these tests, the specimen was deformed to predetermined strains under constraint. Immediately after, the force required to push these deformed samples out of the constraint was measured as a function of time. These measurements were also done on the same servo-hydraulic universal testing machine (Model 8502, INSTRON Co., USA) that was used for all the tests reported in the companion article.[1] The results are shown in Figure 9. Three features are noteworthy. First, there is a measurable

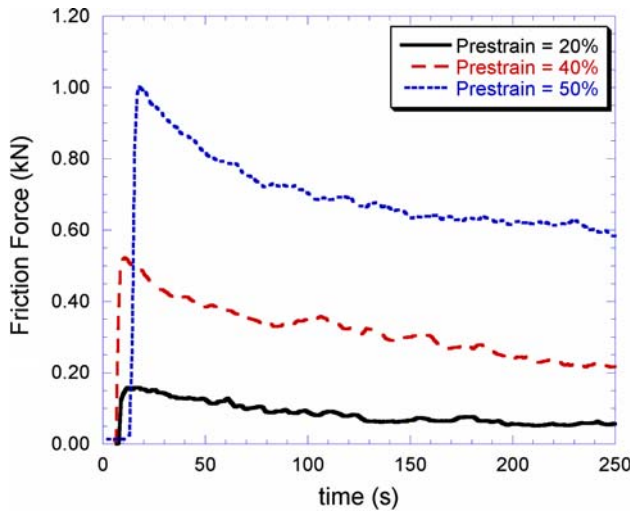

Fig. 9—Residual friction force is plotted as a function of time for samples deformed to three different prestrain levels.

friction force even after the specimen is unloaded. Second, the residual friction increases with increasing prestrain. Finally, the friction force decays with time. These observations cannot be justified on the basis of the homogeneous deformation model. This model cannot predict residual friction in the first place, much less the other features. However, if one allows for collective collapse of cells, one can qualitatively explain the features of Figure 9. Gibson and Ashby[4] have shown that the elastic Poisson's ratio depends largely on the shape of the cells and not the relative density. The collapsed cells within the bands have a higher density and are structurally different from the cells in the starting foam, and so the elastic Poisson's ratio within the band can be expected to be different. There is even a possibility of cell inversion within the bands, and this could lead to a negative elastic Poisson's ratio locally. For these reasons, elastic unloading along the longitudinal direction may not completely unload the transverse elastic stresses. These residual transverse stresses result in the measured friction force. The increase in residual friction with plastic strain is expected, because the volume fraction of material in bands increases with strain. Though the transient drop in friction force is reminiscent of anelastic behavior, it is proposed that the transient is associated with plastic backflow of the foam driven by the residual elastic stresses in the band. Further experiments will be needed to get a clearer mechanistic picture from these results.

There is further evidence (for example, stress drops during constant strain rate tests) suggesting that collective collapse indeed takes place even under constraint. This is also supported by our measurements of density profiles in samples tested with constraint. Figure 10 shows the distribution of relative densities in the foam deformed up to specified strains under constraint. This was calculated by cutting the tested samples into 5-mm sections along the length and measuring densities of those sections. The bimodal distribution of density in these plots suggests that deformation is largely heterogeneous. This is additionally confirmed by macrographic evidence (Figure 5(a), Part I) and by preliminary X-ray radiographic density maps. Both methods reveal the formation of localized regions of high density.

Figure 10 also reveals slight densification of the "unbanded" regions in the foam, particularly during the early stages of deformation. Recent X-ray radiography experiments also indicate that there is marginal densification even outside the bands. Such densification provides a possible explanation for the smaller densification strains observed in constrained tests. Moreover, as pointed out earlier, the bands are not perpendicular to the loading axis again suggesting that the deformation modes are somewhat different with and without constraint, an assumption not made in the heterogeneous model. It appears that minor densification of the foam, as assumed in homogeneous deformation, takes place during constrained deformation. Based on these observations, it is proposed that under constraint the material deforms principally by collective cell collapse, *i.e.*, heterogeneously, but there is small but measurable homogeneous deformation also taking place in tandem.

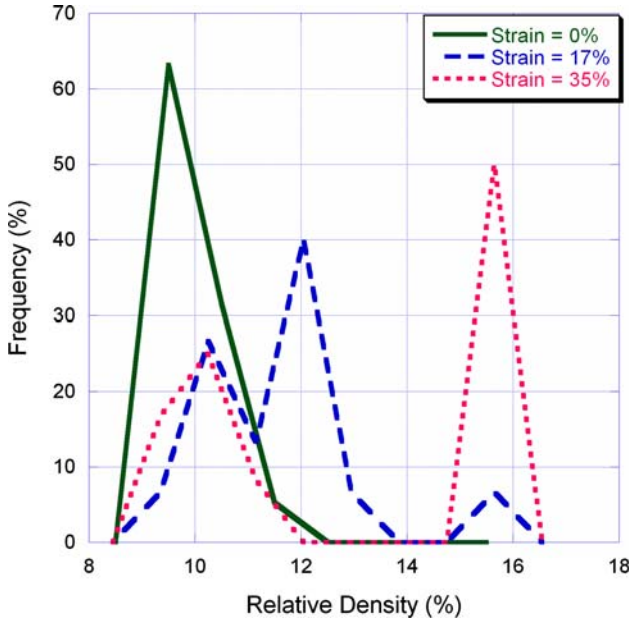

Fig. 10—Distribution of relative densities for foams that have undergone 0, 17, and 35 pct plastic deformation. The figure shows a bimodal distribution of densities suggesting heterogeneous deformation. The peaks centered about a relative density of 10 pct represent the "unbanded" foam, while the peaks at higher densities represent the bands.

The secondary contribution of homogeneous densification to strain hardening is probably not as significant as the frictional contribution.

It is apparent that the foam evolves structurally during deformation. The observed strain hardening depends on the exact manner in which the density distribution evolves with strain. For instance, the premature densification predicted by the homogeneous model is a result of our simplified assumption of structural homogeneity. In fact, this early densification results in the homogeneous model predictions overshooting experiment in Figure 7 for higher density foams. Heterogeneities in the sample cause the plastic instabilities that lead to band formation even in the constrained case where it is not expected. It is quite likely that the triaxial stress state delays the onset of instability leading to homogeneous densification at small strains, whereas the instability invariably sets in due to structural inhomogeneities leading to band formation at larger strains. To verify this and other possibilities, X-ray tomography experiments are presently underway. These experiments are expected to provide a more accurate distribution of density as a function of strain and will confirm the extent to which deformation is homogeneous or heterogeneous.

The role of strain hardening on the fatigue properties is not completely understood and we intend to pursue this aspect of constrained deformation further. It has been argued that the excellent damping properties of metal foams are related to their anelastic nature.[18–20] This property is also expected to affect deformation under cyclic loading. As shown in Figure 9, metal

foams display time-dependent plastic backflow, and this will play an important role in determining the fatigue properties. It was shown in Part I that, during cyclic loading, the rate of strain accumulation is lower in the constrained case. It appears that this is largely related to strain hardening, which leads to a lower effective value of (σ_{max}/σ_p). The observed strain hardening is proposed to be related to friction. Frictional dissipation postpones the onset of stage II in our fatigue results. It will be interesting to conduct cyclic (and monotonic) experiments with a lubricated foam/constraint interface. Such tests will help in isolating the role of friction.

Finally, it needs to be stated that the scatter observed in the data is probably due to the presence of morphological defects such as missing cell walls, voids, wiggles in the cell walls, *etc*., which profoundly influences deformation characteristics of the foams. The influence of cell wall curvatures, wiggles on reduction in modulus, and yield strength is now well recognized.[7,21,22] Inhomogeneous density distribution at mesoscopic scale also exerts considerable influence on compression properties.[23] As a first approximation, we have ignored the influence of these parameters on the deformation characteristics of the foams, but the incorporation of these parameters in the model can be expected to give rise to more realistic predictions.

VII. SUMMARY

In this article, qualitative and quantitative arguments were put forth to justify the mechanisms for strain hardening in metal foams when they are compression tested under lateral constraint. The following summarizes the important points of this work.

1. It was shown that there are two sources of the observed hardening. A change in the stress state (from uniaxial to triaxial) makes deformation more difficult with constraint. Additionally, friction between the deforming foam and the walls of the constraining sleeve also contributes to the observed hardening.
2. The DF yield surface was adopted to evaluate the yield strength under the triaxial loading observed with constraint. The frictional contribution was modeled as a function of the transverse stresses.
3. The transverse stresses were evaluated *via* two deformation models, assuming either heterogeneous or homogeneous deformation of the foam under constraint. In the former model, it was assumed that deformation occurred *via* collective plastic collapse of cells. For the latter, the foam densifies uniformly throughout.
4. The predictions from both models compared favorably with experiment. However, critical experimental evidence such as the dependence of strain hardening rate on the specimen aspect ratio, the presence of a friction force even after the specimen was nominally unloaded, and the macrographic observation of bands, suggests that the material deformed largely by collective cell collapse. There is some evidence that homogeneous deformation also takes place simultaneously, as hinted by the smaller densification strains with constraint.
5. It is evident that friction makes a major contribution to the observed strain hardening behavior and to the sluggish accumulation of strain during fatigue tests.

REFERENCES

1. M. Kolluri, S. Karthikeyan, and U. Ramamurty, DOI: 10.1007/s11661-007-9245-z.
2. A. Harte, N. Fleck, and M. Ashby: *Acta Mater*., 1999, vol. 47, pp. 2511–24.
3. A. Evans, J. Hutchinson, and M.F. Ashby: *Progr. Mater. Sci*., 1998, vol. 43, pp. 171–221.
4. L. Gibson and M. Ashby: *Cellular Solids—Structure and Properties*, 2nd ed., Cambridge University Press, Cambridge, United Kingdom, 1997, pp. 175–281.
5. H. Bart-Smith, A. Bastawros, D. Mumm, A. Evans, D. Sypeck, and H. Wadley: *Acta Mater*., 1998, vol. 46, pp. 3583–92.
6. E. Maire, A. Emoutaouakkil, A. Fazekas, and L. Salvo: *MRS Bull*., 2003, vol. 28, pp. 284–89.
7. E. Andrews, W. Sanders, and L. Gibson: *Mater. Sci. Eng. A*, 1999, vol. A270, pp. 113–24.
8. P. Kenesei, C. Kadar, Z. Rajkovits, and J. Lendvai: *Scripta Mater*., 2004, vol. 50, pp. 295–300.
9. V. Deshpande and N. Fleck: *J. Mech. Phys. Sol*., 2000, vol. 48, pp. 1253–83.
10. G. Gioux, T. McCormack, and L. Gibson: *Int. J. Mech. Sci*., 2000, vol. 42, pp. 1097–1117.
11. R. Miller: *Int. J. Mech. Sci*., 2000, vol. 42, pp. 729–54.
12. D. Ruan, G. Lu, and B. Wang: *WIT Trans. Eng. Sci*., 2005, vol. 49, pp. 437–49.
13. T. Triantafillou, J. Zhang, T. Shercliff, L. Gibson, and M. Ashby: *Int. J. Mech. Sci*., 1989, vol. 31, pp. 665–78.
14. M. Silva, W. Hayes, and L. Gibson: *Int. J. Mech. Sci*., 1995, vol. 37, pp. 1161–77.
15. C. Chen, T. Lu, and N. Fleck: *J. Mech. Phys. Sol*., 1999, vol. 47, pp. 2235–72.
16. J. Grenestedt: *J. Mech. Phys. Sol*., 1998, vol. 46, pp. 29–50.
17. J. Zhang, N. Kikuchi, V. Li, A. Yee, and G. Nusholtz: *Int. J. Impact Eng*., 1998, vol. 21, pp. 369–86.
18. J. Banhart: *Progr. Mater. Sci*., 2001, vol. 46, pp. 559–632.
19. C.S. Liu, Z. Zhu, F. Han, and J. Banhart: *Phil. Mag. A*, 2000, vol. 80, pp. 1085–92.
20. I. Golovin and H.-R. Sinning: *Mater. Sci. Eng. A*, 2004, vol. 370, pp. 504–11.
21. U. Ramamurty and A. Paul: *Acta Mater*., 2004, vol. 52, pp. 869–76.
22. Y. Sugimura, J. Meyer, M. He, H. Bart-Smith, J. Grenestedt, and A. Evans: *Acta Mater*., 1997, vol. 45, pp. 5245–59.
23. J. Beals and M. Thomson: *J. Mater. Sci*., 1997, vol. 32, pp. 3595–3600.